Direct calibration using atmospheric particles and performance evaluation of PSM 2.0 for sub-10 nm particle measurements

Yiliang Liu[1,2], Arttu Yli-Kujala[2], Fabian Schmidt-Ott[2], Sebastian Holm[2], Lauri Ahonen[2], Tommy Chan[2], Joonas Enroth[3], Joonas Vanhanen[3], Runlong Cai[4], Tuukka Petäjä[2], Markku Kulmala[2], Yang Chen[1], and Juha Kangasluoma[2]

[1]Chongqing Institute of Green and Intelligent Technology, CAS, Chongqing, 400714, China
[2]Institute for Atmospheric and Earth System Research / Physics, University of Helsinki, Helsinki, 00014, Finland
[3]Airmodus Ltd., Helsinki, 00560, Finland
[4]Department of Environmental Science & Engineering, Fudan University, Shanghai, 200438, China

Correspondence to: Juha Kangasluoma (juha.kangasluoma@helsinki.fi), and Yang Chen (chenyang@cigit.ac.cn)

Abstract. Particle Size Magnifier is widely used for the measuring nano-sized particles. Here we calibrated the newly developed Particle Size Magnifier version 2.0 (PSM 2.0). 1-10 nm particles with different compositions were used, including metal particles, organic particles generated in the laboratory and atmospheric particles collected in Helsinki and Hyytiälä, respectively. Noticeable difference among the calibration curves was observed. Atmospheric particles from Hyytiälä required higher DEG supersaturation to be activated compared to metal particles (standard calibration particles) and other types of particles. This suggests that chemical composition differences introduce measurement uncertainties and highlight the importance of in-situ calibration. The size resolution of PSM 2.0 was characterized using metal particles. The maximum size resolution was observed at 2-3 nm. PSM 2.0 was then operated in Hyytiälä for ambient particle measurements in parallel with a Half-mini Differential Mobility Particle Sizer (DMPS). During new particle formation (NPF) events, comparable total particle concentrations were observed between Half-mini DMPS and PSM 2.0 based on Hyytiälä atmospheric particle calibration. Meanwhile, applying the calibration with metal particles to atmospheric measurements would cause an overestimation of 3-10 nm particles. In terms of the particle size distributions, similar patterns were observed between DMPS and PSM when using the calibration of Hyytiälä atmospheric particles. In summary, PSM 2.0 is a powerful instrument for measuring sub-10 nm particles and can achieve more precise particle size distribution measurements with proper calibration.

1 Introduction

Particle Size Magnifier (PSM) is a powerful instrument for measuring the size distributions of nanoparticles. It finds extensive applications across various research domains, such as atmospheric studies (Kulmala et al., 2013; Winkler et al., 2008; Yao et al., 2018), nano material research (Liu et al., 2024; Wlasits et al., 2020), combustion research (Rönkkö et al., 2017), health sciences, etc. The prototype instrument was developed by Kogan et al. in 1960 (Kogan and Burnasheva, 1960), followed by a series of different types of designs (Kim et al., 2003; Okuyama et al., 1984; Sgro and Fernández de la Mora, 2004). In 2011,

PSM version 1.0 was commercialized by Airmodus Ltd. (Vanhanen et al., 2011), and became available for research groups worldwide. In 2023, Airmodus Ltd. unveiled PSM version 2.0, boasting several enhancements over its predecessor (Sulo et al., 2024). These improvements include an expanded measurement size range, enhanced durability, higher instrument stability,

35 and improved user-friendliness.

The activation of particles in PSM relies on heterogeneous nucleation under varying supersaturation of diethylene glycol (DEG) vapor. As DEG supersaturation increases, smaller particles become activated. The minimum particle size that can be activated is around 1 nm, at the brink of DEG homogeneous nucleation (Iida et al., 2011). However, the performance of PSM, as well as some other condensation-based instruments, is influenced by many factors. A review paper that summarizes and discusses

40 the uncertainties is published recently (Kangasluoma et al., 2020). The uncertainties in particle activation come from the particle properties, ambient conditions, and instrument setups, etc. Environmental conditions such as humidity and air pressure can result in the offset between the DEG supersaturation and particle activation, and thereby introduce uncertainties for the measured particle size distributions (Liu et al., 2020). As the relative humidity (RH) of the carrier gas increases, nanoparticles can be activated at a lower DEG saturator flow rate, leading to a shift in the cut-off size towards smaller particles (Kangasluoma

45 et al., 2013, 2016b). This phenomenon is attributed to the hygroscopic properties of nanoparticles and vapor-particle interactions due to hydrogen bonding (Keshavarz et al., 2020b; Toropainen et al., 2021). The charging state of particles also affects their activation. Charged particles tend to activate at a lower saturator flow rate compared to neutral particles (Kangasluoma et al., 2016a; Keshavarz et al., 2020a), because the charge on a particle reduces the energy barrier for DEG condensation.

50 Among all the influencing factors, the chemical composition of particles exerts the strongest influence on particle detection (Kulmala et al., 2007). Metal and salt particles typically exhibit higher detection efficiency by PSM compared to organic particles (Kangasluoma et al., 2014; Liu et al., 2022). The standard practice involves calibrating the PSM in a laboratory using metal particles and then employing it for measuring particles with complex and unknown compositions (Lehtipalo et al., 2021). This process inherently introduces some uncertainties due to the variation in chemical composition of particles used for

55 calibration and measurement. Calibrating the PSM with particles of the same chemical composition as those being measured can minimize measurement uncertainties (Ahonen et al., 2017). However, applying this approach can be challenging, as it requires specific and directly relevant particle sources and a HR-DMA, which are not always readily available. Additionally, the measured nanoparticles often have complex compositions and low concentrations, making it difficult to generate particles with identical compositions in the laboratory.

60 In this study, we performed calibration on PSM 2.0 using different kinds of particles, including commonly-used metal particles, organic particles, as well as the direct calibration using atmospheric particles. In addition, PSM 2.0 was operated in parallel with a DMPS (Differential Mobility Particle Sizer) for the measurement of ambient particles. The results help us to have a better understanding about the effects of particle composition as well as the sizing accuracy of PSM 2.0.

2 Methods

2.1 Working principle of PSM 2.0

The working principle of PSM 2.0 is similar to that of its predecessor, PSM 1.0, involving a two-step activation and growth process for nanoparticles. First, particles are activated using supersaturated DEG vapor, where increased DEG supersaturation enables the activation of smaller particles. In the second step, the activated particles grow to an optically detectable size within a butanol-based CPC. The size distributions can be calculated through a proper data inversion process, and in this study the step inversion method was used (Cai et al., 2018b; Chan et al., 2020).

PSM 2.0 offers several improvements compared over PSM 1.0. Firstly, it features a more stable internal flow field, achieved by controlling DEG supersaturation through two distinct flows: a wet flow carrying DEG vapors and a dry flow of particle-free compressed air (Attoui et al., 2023). The wet flow rate can be adjusted between 0.05 and 1.90 L min^{-1}, while maintaining a stable total flow rate of wet and dry flows. The enhanced stability and precision in the flow system lead to more predictable dilution factors under different saturator flow rates and minimize concentration fluctuations caused by changing flow rates. Secondly, PSM 2.0 offers a broader range of DEG supersaturation adjustments than PSM 1.0. By controlling the ratio of dry to wet flow rates, it enables to achieve a lower supersaturation level, which is crucial for extending the instrument's size measurement range.

2.2 PSM 2.0 calibration

3
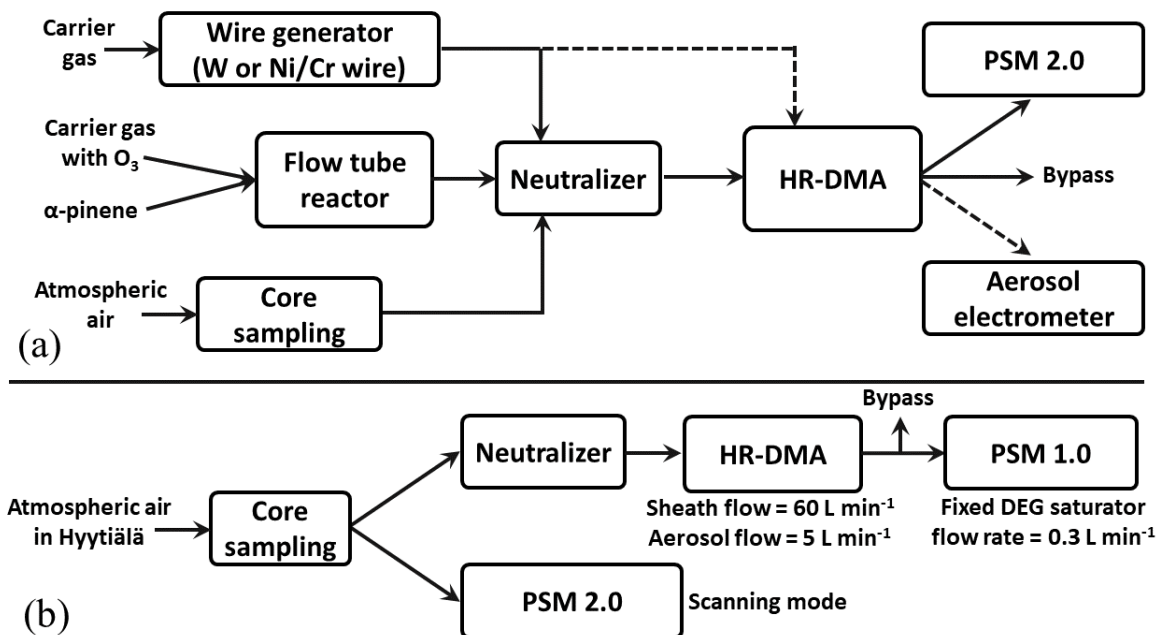
Figure 1. (a) A schematic diagram illustrating the calibration of PSM 2.0 using metal particles (tungsten and nickel/chromium particles), organic particles (alpha-pinene oxidation particles), and atmospheric particles collected in Helsinki and Hyytiälä. The flow configuration is detailed in Table 1. (b) PSM 2.0 operated in parallel with a DMPS to measure atmospheric particles in Hyytiälä. The HR-DMA operated with an aerosol flow rate of 5 L min⁻¹ and a sheath flow rate of 60 L min⁻¹.

85 A schematic diagram for PSM 2.0 calibration is displayed in Fig. 1(a). Different types of particles were used, including tungsten metal particles, nickel/chromium particles, alpha-pinene oxidation particles, Helsinki atmospheric particles and Hyytiälä atmospheric particles (Table 1). Metal particles generated in wire generators are commonly used for PSM calibration, because they provide appropriate concentrations and their activation behaviour is similar to that of salt particles, which are assumed to be one of the major components of ambient aerosols (Kangasluoma et al., 2014, 2015). For the tungsten particle generation,

90 nitrogen was used as the carrier gas, while synthesized air was used for Ni/Cr particle generation. Tungsten particles ranged in size from 1.2 to 20.3 nm across 68 sizes, whereas Ni/Cr particles ranged from 1.2 to 14.0 nm across 10 sizes. Organic particles were generated in the flow tube reactor through the reaction of alpha-pinene with ozone. The generation method was comparable to that mentioned in a previous study (Li et al., 2022). The particles, ranging in size from 1.6 to 9.4 nm, were classified into 10 sizes and used for PSM 2.0 calibration. The compositional differences between laboratory-generated particles

95 and atmospheric particles have been the main source of uncertainty in PSM measurements. Ambient particle compositions vary significantly across different locations, highlighting the value of performing direct calibration using atmospheric particles. A burst increase in sub-10 nm particle concentrations was observed during NPF events in Helsinki and Hyytiälä, with atmospheric particles being sampled directly for the calibration of PSM 2.0.

~~We also used atmospheric particles for PSM 2.0 calibration. Burst increase of sub-10 nm particle concentrations was observed~~

100 ~~during NPF events in Helsinki and Hyytiälä. The standard temperature settings by the manufacturer were used for all calibration experiments, and one more calibration was performed under boosted temperature setting in Hyytiälä. The temperatures for both the standard and boosted settings are displayed in Table 2.~~

After the particle generation, the aerosol flow passed through a neutralizer (Ni-63) before undergoing size classification by an HR-DMA (Cai et al., 2018a; Fernández de la Mora, 2017). Some of the metal particles were self-charged, so the neutralizer

105 was removed when using sub-3 nm tungsten to calibrate the instrument. It will help to eliminate the effects of neutralizer ions of the calibration. High sheath flow rates were generally used for classifying metal particles to enhance their monodispersity in the laboratory experiments (Table 1). ~~Conversely, a lower~~ A decreased DMA sheath/aerosol flow rate ratio of ~~(~~60/5 L min⁻¹/ L min⁻¹~~)~~ was used for the classification of atmospheric particles ~~to increase their concentration signal.~~, which would help to increase the penetration efficiency of nanoparticles passed through the DMA, and obtain a sufficient concentration for

110 calibration.

After the HR-DMA classification, the ~~monodispersed~~ classified particles were directed to PSM 2.0 and an Aerosol Electrometer (AEM) at equal flow rates of 2.7 L min⁻¹. PSM 2.0 was operated in scanning mode, with the DEG saturator flow rate(s) repeatedly increasing and decreasing between 0.05 and the peak value (usually 1.9 L min⁻¹). Particle concentrations at different DEG saturator flow rates were recorded. The AEM was only used for the calibration using metal particles and organic

115 particles, when particle concentrations exceeded 500 cm⁻³. For the calibration using atmospheric particles, the particle

concentrations after the DMA classification were very low (<100 cm^{-3}). The concentrations were lower than the background noise concentrations from the AEM. In this case, tThe identification of true particle concentrations without AEM relies on the concentrations measured at different DEG saturator flow ratesis based on the . plateau concentrations by PSM 2.0 at high DEG saturator flow rates. For particles larger than 2 nm, plateau concentrations measured at high DEG saturator flow rates represented the true particle concentrations.

The standard temperature settings by the manufacturer were used for all calibration experiments, and one more calibration was performed under boosted temperature setting in Hyytiälä. The temperatures for both the standard and boosted settings are displayed in Table 2. The standard temperature setting established a condenser temperature of 10°C to reduce the potential co-condensation between diethylene glycol (DEG) and water molecules at peak DEG saturator flow rates. The saturator temperature was carefully adjusted to ensure that the scanning DEG saturator flow rate (from 0.05 to 1.90 L min^{-1}) could activate particles both near 1 nm and larger than 10 nm. The boosted temperature setting approached the threshold for DEG homogeneous nucleation at peak DEG saturator flow rates, enhancing PSM's detection efficiency for particles closing to 1 nm, meanwhile reducing the upper size limit.

Table 1. Summary of particles used for PSM 2.0 calibration. The particles were either generated in the laboratory using particle generators or sampled from atmosphere during NPF events.

#	Particle source	Particle type	Carrier gas	Neutralizer	HR-DMA sheath flow (L min^{-1})	HR-DMA aerosol flow (L min^{-1})	Particle size range (nm)	Aerosol electrometer
1	Wire generator	Tungsten particles	N$_2$	√	300, 145, 100	10, 6	1.2-20.3	√
2	Wire generator	Nickel/chromium particles	Synthesized air	√	200	10	1.2-14.0	√
3	Organic particle generator	Alpha-pinene oxidation particles	Synthesized air	√	150	5.4	1.6-9.4	√
4	Helsinki ambient air	Ambient particles	Atmospheric air	√	60	5	2-11	
5	Hyytiälä ambient air	Ambient particles	Atmospheric air	√	60	5	2.5-11	

2.3 Campaign measurement

After the calibration, PSM 2.0 was operated in parallel with a DMPS to measure ambient particles in Hyytiälä (Fig. 1(b)). This lasted for three weeks from 1 May to 21 May, 2024. The instrument configurations are displayed in Table 2. Both the PSM 2.0 and DMPS used core-sampling method, with a carrier gas flow rate of 10.0 L min^{-1} in the main sampling tube. PSM 2.0 was operated under the scanning mode, with the DEG saturator flow rate increasing from 0.05 to 1.80 L min^{-1}, and then

decreasing. Each DEG scan took 4 minutes. A step inversion method was used for PSM 2.0 data inversion, based on calibration files using different types of particles.

Table 2. Configuration settings for PSM 2.0 and DMPS during the ambient particle measurement in Hyytiälä.

Instrument	Core sampling	Neutralizer	Mode	Setting	Time per scan	Size bins
PSM 2.0	√		DEG scanning from 0.05 to 1.80 L min^{-1}	Inlet/saturator/condenser = 40/71/10 (°C) *	240 s	6-9
DMPS	√	√	Voltage scanning from 100 to 2000 V	Sheath/aerosol = 60:5(L min^{-1})	220 s	10

* Under the boosted PSM temperature setting, the temperature of the condenser was 7 °C.

140 For DMPS (Kangasluoma et al., 2018), after the core-sampling, aerosol flow passed through a Ni–[63] neutralizer at a flow rate of 5.0 L min^{-1}. Particles were then size-classified by a ~~half~~Half-mini DMA (sheath flow rate of 60 L min^{-1}). PSM 1.0 was used as the concentration detector of DMPS, which operated at a fixed DEG saturator flow rate of 0.3 L min^{-1} (with a background concentration of almost 0 cm^{-3}). We used the DMPS inversion method as displayed in a previous study (Jiang et al., 2011). An equivalent length of 1.8 m was used to correct the diffusion losses inside the neutralizer. A charging steady state was assumed

145 to be achieved inside the neutralizer (Wiedensohler and Fissan, 1991). The transmission function of ~~half~~Half-mini DMA was obtained from a previous study (Cai et al., 2018b). The detection efficiencies of different sized particles by the detector (PSM 1.0) were calibrated using alpha-pinene oxidation particles.

2.4 Data processing

2.4.1 Detection efficiency curve

150 For particles of a certain size, their detection efficiencies (η) at different DEG saturator flow rates were calculated based on the ratios of the concentrations measured by PSM 2.0 and actual concentrations. For metal particles and organic particles, the actual concentrations were typically higher than 1000 cm^{-3}, and could be measured by the AEM. However, in terms of ambient particles after DMA classification, their concentrations were identified based on the assumption that a stable plateau observed under high DEG saturator flow rates represented the real particle concentrations. The detection efficiencies under different

155 DEG saturator flow rates were fitted using the following Eq. (1):

$$\eta = \frac{1}{\left(1+e^{(-a\cdot(s-b))}\right)} \ , \tag{1}$$

where s is the DEG saturator flow rate, a and b are fitting parameters.

2.4.2 Kernel function curve

The Kernel function represents the derivative of the fitted detection efficiency curve with respect to the saturator flow rate (Cai

160 et al., 2018b). The peak point of the Kernel function helps to establish the correlation between the DEG saturator flow rates and the corresponding cut-off sizes. Additionally, the width of the Kernel function suggests if the activation of particles

6

happened within a narrow DEG saturator flowrate variation or a wide range. The sizing resolution in DEG saturator flow rate space ($Res(S^*)$) of PSM 2.0 can be evaluated, accordingly:

$$Res(S^*) = \frac{S^*}{\Delta S} \qquad (2)$$

165 where S^* is the saturator flow rate corresponding to the peak point of the Kernel function, and ΔS is the full width at half maximum of the Kernel function peak.

Several factors influence $Res(S^*)$, including the temperature configuration of the PSM, the uniformity and stability of DEG supersaturation within the instrument, and the uniformity of the size and chemical composition of the particles (Fernández de la Mora et al., 2022). ~~Meanwhile, the incomplete detection efficiency curves and Kernel functions would introduce some~~

170 ~~uncertainties in the calculated $Res(S^*)$.Generally, increasing the temperature difference between the PSM's saturator and condenser results in a dramatic change in supersaturation,~~ In general, improving the uniformity and stability of DEG supersaturation within the PSM would enhance detection efficiency curve's sharpness, thereby enhancing the $Res(S^*)$. Conversely, variations in particle composition and poor monodispersity of particles can broaden the measured kernel function peaks, leading to a decrease in $Res(S^*)$. This study did not attempt to quantify the impact of these factors. Instead, we only

175 ~~used the standard temperature settings by Airmodus and~~ characterized PSM 2.0's $Res(S^*)$ using metal particles under the standard temperature setting.

~~However, t~~The $Res(S^*)$ alone cannot demonstrate the sizing capability of the PSM 2.0, because the relationship between particle sizes and DEG saturator flow rates is not linear. In terms of metal particles, slight variations in the saturator flow rate would lead to significant fluctuations in the corresponding cut-off sizes (Fig. 5). To address this, we cited the DMA's definition

180 of size resolution, by replacing the DEG saturator flow rate in the Kernel function with the corresponding cut-off size (based on the calibration curve). After that, we calculated the size resolution of PSM ($Res(d_p^*)$) at specific particle size (d_p^*):

$$Res(d_p^*) = {d_p^*}\big/{\Delta d_p} = Res(S^*)\frac{d_p^*}{S^*}\frac{1}{-f'[S^*]}, \qquad (3)$$

where $f[S^*]$ is the fitted function displaying the cut-off size at the saturator flow rate of S^*. $f'[S^*]$ suggests the derivation of the fitted function at the DEG saturator flow rate of S^*. ~~In general, T~~the size resolution of PSM is related to the $Res(S^*)$~~DEG~~

185 ~~resolution~~, and also influenced by the calibration curve. The physical meaning of $Res(d_p^*)$ is the size range corresponding to the particle activation at a given DEG saturator flow rate. Higher size resolution means that each DEG saturator flow rate corresponds to a narrower size range near the cut-off size, and vice versa. Please refer to SI for the detailed derivation process.

2.4.3 Calibration curve

The calibration curve was based on the peak points of different-sized particles in the Kernel functions, and showed a one-to-

190 one correspondence between the DEG saturator flow rate and cut-off size. Various types of particles were used to calibrate the PSM 2.0, resulting in different calibration curves. This ~~relationship~~ calibration curve is crucial for PSM 2.0 data inversion. In terms of the step inversion method, the size resolution of the PSM 2.0 at each DEG saturator flow rate is assumed to be infinite.

the The activation of particles larger than the cut-off size are assumed to be 100%, while for particles smaller than the cut-off size, their activation efficiencies are assumed to be 0%.

3 Results and discussion

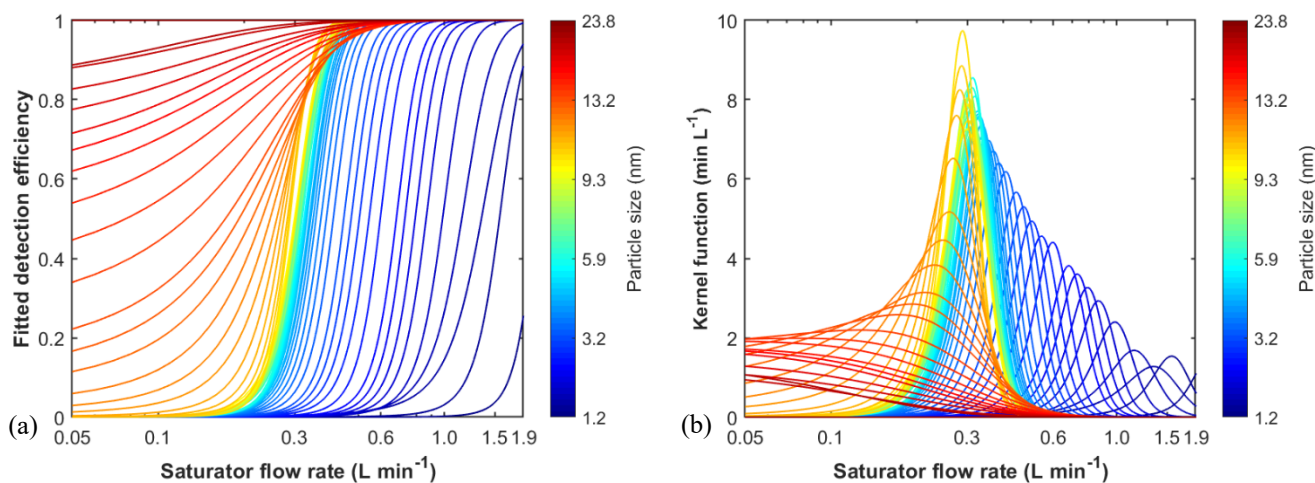### 3.1 PSM 2.0 Calibration using metal particles

Figure 2. (a) The fitted detection efficiency curves according to the calibration using tungsten particles. (b) The calculated Kernel function curves according to the fitted detection efficiencies curves.

Figure 2(a) presents the detection efficiency curves for different sized tungsten particles. The detection efficiency increasing from 0% to plateau values (close to 100%) can be found as the DEG saturator flow rate increasing. The detection efficiency curves can be divided into two groups. The first group is for sub-10 nm particles, where the fitted detection efficiency curves maintain a consistent and approximate parallel pattern. where the detection efficiency curves run approximately parallel to each other. This parallel pattern suggests that particle size is a key factor influencing activation. As particle size increase, a leftward shift in the detection efficiency curve is observed. The detection efficiency increasing from 0% to plateau values (close to 100%) can be found as the DEG saturator flow rate increasing. Plateau values close to 100% were observed because the dilution factor under different DEG saturator flow rates were well calibrated in the PSM 2.0.

The second group is for particles larger than 10 nm. The curves deviate from the parallel pattern and begin to flatten as size increases. A plausible explanation is that the activation of particles above 10 nm is not solely determined by the DEG saturator flow rate but also by the downstream CPC. Particles larger than 10 nm start to be activated by the CPC with finite and increasing detection efficiencies. It hinders the establishment of a one-to-one relationship between each DEG saturator flow rate and its corresponding cut-off size.

215 ~~The second group is for particles larger than 10 nm, where the detection efficiency curves start to flatten out, with increased detection efficiencies observed at the lowest saturator flow rate (0.05 L min⁻¹). This is because the activation of particles larger than 10 nm started to be influenced by the activation in the down-stream CPC.~~

~~Due to variations in detection efficiency curves for particles of varying sizes, PSM 2.0 can theoretically detect particles ranging from 1 to 20 nm. However, calibrating particles within the 10-20 nm range yields higher uncertainties.~~

In the calibration by using particles larger than 10 nm, we found the ~~c~~Concentrations measured by the AEM ~~were gradually~~started exceed those of ~~higher than~~ PSM 2.0, with the difference increasing to 30% as particle size approached 20

220 nm~~as particle size closing to 20 nm~~. This discrepancy ~~probably~~ likely arises from the presence of ~~multiply~~ charged particles after the DMA classification, which can ~~,~~ ~~lead~~ing to an overestimation in concentrations by AEM. Consequently, in this size range, the concentrations measured by PSM 2.0 at the high DEG flow rates were adopted as the actual particle concentrations and used to plot the detection efficiency curves in Fig. 2(a).

$Res(S^*)$ of PSM 2.0 was calculated based on the Kernel function as displayed in Fig. 2(b). Notably, the $Res(S^*)$ remained

225 stable for particle ~~sizes~~between 2.0 ~~to~~and 10.0 nm, approximately at 3 (Fig. 3). The decreasing trend in the $Res(S^*)$~~resolution~~ for sub-2 nm particles may come from the changes in chemical compositions within this size range. To get a high concentration of sub-2 nm particles for instrument calibration, a higher heating power was used by the wire generator, which could ~~possibly~~ increase the fraction of organic components in sub-2 nm metal particles ~~in nanoparticles~~. When sub-2 nm particles contain a mixture of metal and organic components, their activation corresponds to a broader range of DEG saturator flow rates. This

230 leads to a flattening of the detection efficiency curve and a reduction in measured $Res(S^*)$. For particles larger than 10 nm, we also observed a decrease in the $Res(S^*)$. As discussed above, the activation of 10-20 nm particles is commonly influenced by the DEG saturator flow rate and the downstream CPC, leading to a flattening of the detection efficiency curves and a reduction in the $Res(S^*)$.

For sub-3 nm particles, the $Res(S^*)$ of PSM 2.0 were quite comparable with PSM 1.0 (Cai et al., 2018b). In 3 to 4 nm size

235 range, a decrease in the $Res(S^*)$ can be found for PSM 1.0, whereas for PSM 2.0, the $Res(S^*)$ remained stable till 10 nm. PSM 2.0 showed a higher $Res(S^*)$ than PSM 1.0 possibly because PSM 2.0 ensures a more stable flow field and enables more precise and uniform control over DEG supersaturation. The PSM 2.0 can reach a much lower DEG supersaturation compared to the PSM 1.0, making it more suitable for measuring particles in the 3 to 10 nm range.
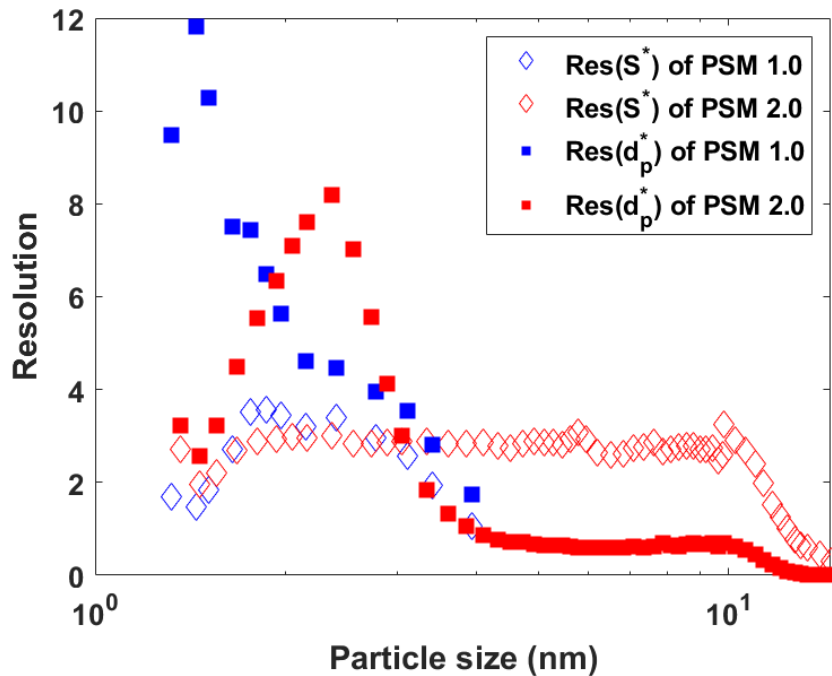
Figure 3. Resolution in DEG saturator flow rate ($Res(S^*)$) and size resolution ($Res(d_p^*)$) for both PSM 2.0 and PSM 1.0. The calculations are based on metal particles classified by an HR-DMA. Commercial temperature settings were used for both instruments. The $Res(S^*)$ of PSM 1.0 are cited from (Cai et al., 2018a).

The size resolution ($Res(d_p^*)$) of PSM 2.0 is a key factor in demonstrating its sizing ability for different particle sizes. Here, we compared the size resolution of PSM 2.0 with that of PSM 1.0. Since the working principle of the PSM is based on particle-vapor interaction under varying DEG supersaturation, this process is strongly influenced by the composition of the seed particles.

were also compared with PSM 1.0In general, higher $Res(d_p^*)$ were observed for small particles for bothe PSM 1.0 and 2.0. For PSM 1.0, a decreasing trend in size resolution was observed as particle size increased. For PSM 2.0, the peak size resolution was observed at around 2.2 nm. The paek resolution was higher than 8, which is comparable or even higher than the DMA's resolution in this size (Cai et al., 2018a). As mentioned above, tThe decrease in $Res(d_p^*)$size resolution for particles smaller than 2.2 nm is similar to the decrease in $Res(S^*)$DEG resolution, as metal particles produced in the wire generator were contaminated by more organic impurities. For particles larger than 4 nm, the size resolution of PSM 2.0 was stable but was lower than 1. In summary, tThough PSM 2.0 expanded the size measurement range from 4 nm of PSM 1.0 to above 10 nm, but the size resolution on 4-10 nm particles was low (<1). This result provides useful insights into the size bin selection for the PSM 2.0. For sub-3 nm particles, smaller size bins are recommended since PSM has higher size resolution in this range, while for particles in the 3 to 10 nm range, larger size bins are advisable.

For particles larger than 10 nm, the size resolution further decreased, indicating larger sizing uncertainties.

10

For particles larger than 10 nm, the size resolution decreases further, resulting in greater sizing uncertainties. In summary, based on calibrations with various-sized metal particles, 10 nm is recommended as the upper size limit for PSM 2.0. This recommendation stems from the higher size resolution of PSM 2.0 in the sub-10 nm range and the fact that particles larger than 10 nm begin to be activated by the CPC.

3.2 PSM 2.0 calibration with ambient particles

### 3.2.1 Ambient particles in Helsinki
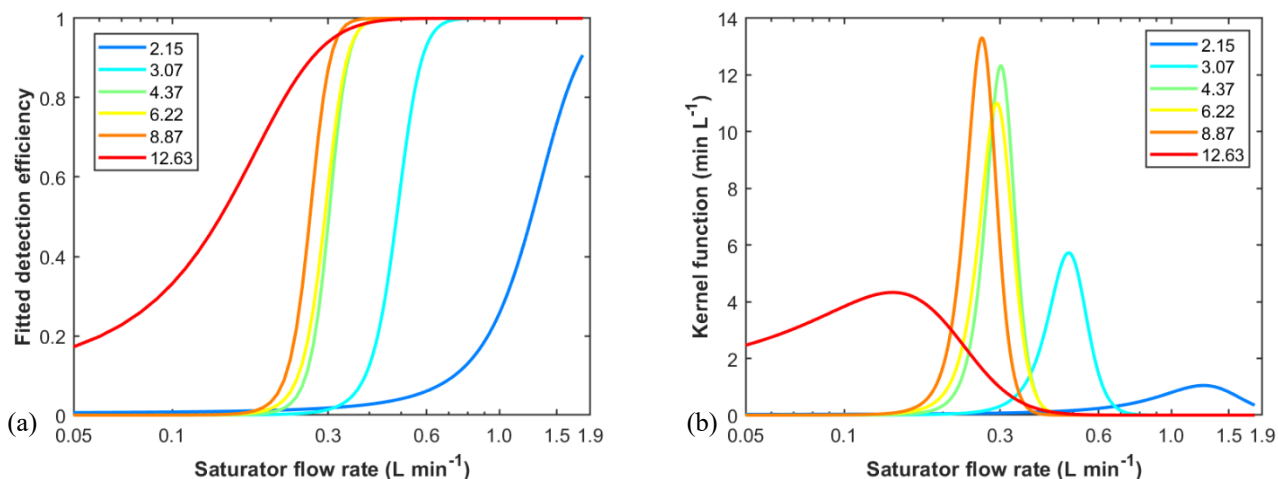
Figure 4. PSM 2.0 calibration based on the ambient particles collected in Helsinki during an NPF event on 18 February. (a) Detection efficiency curves of different sized particles. (b) Kernel function curves of different sized particles.

Two NPF events in Helsinki were identified on 18 and 19 February, respectively. The size-resolved detection efficiency curves are displayed in Fig. 4 (a). Similar to the results of metal particle calibration, the detection efficiency curves of Helsinki ambient particles also moved toward left side, as particle size increasing. The corresponding Kernel function is plotted (Fig. 4 (b)). The main challenge of performing direct calibration using atmospheric particles is the low concentrations (Fig. S1). During NPF events, the size-resolved concentrations of ambient particles were several magnitudes lower than those from the particle generator. After DMA classification, the concentrations of sub-2 nm particles approached 0 cm^{-3}. When concentrations are very low, it becomes difficult to identify the actual values for calibration. Therefore, only particles larger than 2 nm were used for PSM 2.0 calibration.

~~In general, for particles larger than 3 nm, the detection efficiency curves can be well fitted, because a plateau value in the detection efficiency curve can be well identified. However, for sub 3 nm particles, especially for sub 2 nm particles, the particles' concentrations were low. Therefore, only particles larger than 2 nm were used for plotting the PSM 2.0 calibration curves. The detection efficiency curves moved toward left side, as particles' size increased. The Kernel function was also plotted (Fig. 4 (b)).~~

11

280   We ~~further~~ compared the calibration ~~results~~ curves for ~~different~~ all types of particles (Fig. 5). Overall, the calibration curves of metal particles, by using tungsten and Ni/Cr particles, are comparable. ~~For organic particles,~~ Some differences are observed between metal particles and organic particles. ~~T~~the ~~activation of~~ sub-4 nm organic particles needs higher DEG saturator flow rate compared to metal particles~~.~~ ~~However, for particles larger than 4 nm, the activation is slightly lower than metal particles.~~ This result is consistent with some previous studies that the activation of organic particles by PSM 1.0 will need higher DEG

285   saturator flow rates (Kangasluoma et al., 2014). For particles larger than 4 nm, the calibration curve of organic particles is comparable or slightly lower than metal particles.

    For atmospheric particles sized between 2-4 nm, the activation of Helsinki ambient particles ~~required a slightly higher DEG saturator flow rate than for~~is comparable with metal particles. ~~Whereas opposite trend was observed for particles larger than 4 nm~~The activation of particles larger than 4 nm will need lower DEG saturator flow rates, which could be related to the higher

290   RH in the ambient atmosphere. The PSM detection efficiency increases with increasing relative humidity (Kangasluoma et al., 2013). Overall, the difference in the calibration curves between metal particles and Helsinki ambient particles is not substantial,~~Our experiments~~ which further confirmed the validity of using metal particles for PSM calibration, and subsequently using the PSM 2.0 to measure atmospheric particles in Helsinki. However, the composition of ambient particles can vary significantly between different cities, as the sources of nucleation mode particles and the mechanisms of new particle

295   formation (NPF) can differ. More direct calibration experiments using different urban atmospheric particles are strongly recommended.
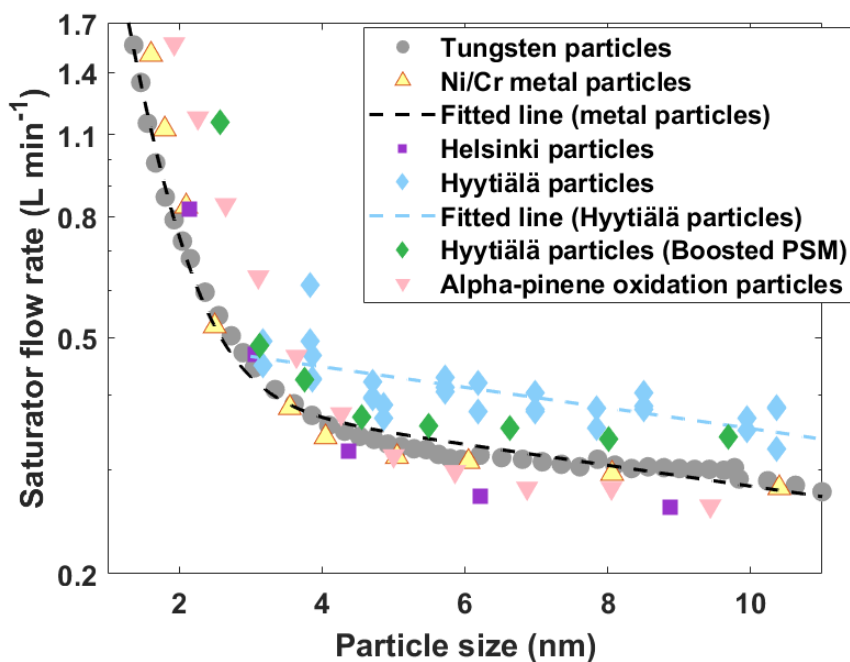
Figure 5. The relationship between DEG saturator flow rates and the corresponding cut-off sizes. The calibrations curves were plotted based on different types of particles, including metal particles, organic particles, and ambient particles collected in different places.

3.2.2 Ambient particles in Hyytiälä

Hyytiälä's atmospheric particles have also been used for PSM 2.0 calibration (Fig. S2-S3). A total of 6 NPF events were identified in Hyytiälä, on 5, 6, 10, 11, 12 March and 4 April, respectively. Among these, 5 events were used to calibrate PSM 2.0 under standard temperature settings, except the event on 4 April, that was used to calibrate the boosted PSM 2.0, with the condenser temperature of 7°C. The fitted detection efficiency curves based on different-sized particles and the raw data are given in the SI. Only the result of particles larger than 3 nm were used for the calibration was used for plotting the calibration curve (Fig. 5), due to the low concentrations of sub-3 nm particles.

Notably, a higher saturator flow rate was is needed for the activation of Hyytiälä ambient particles, compared with metal particles, organic particles, or the ambient particles in Helsinki. It suggests the composition difference between Hyytiälä ambient particles and other types of particles, which would cause the difference in their activation in PSM 2.0. The ambient particles in Hyytiälä predominantly comprised of organic components, but is the properties of organic particles in Hyytiälä may different from the alpha-pinene oxidation particles generated in the lab. A plausible explanation is that organic particles formed through alpha-pinene oxidation were highly oxidized, resulting in activation behavior similar to that of metal particles. In contrast, atmospheric particles from Hyytiälä could had a lower oxidation state, and would require a higher DEG supersaturation for activation. This observation conclusion was further corroborated by the boosted PSM 2.0 experiment. By increasing the temperature difference between the saturator and condenser, the calibration curve of Hyytiälä ambient particles moves toward to the calibration curve of metal particles under standard temperature setting.

In summary, the calibration curves for different particle types show some variation. Metal particles, Helsinki ambient particles, and alpha-pinene oxidation particles larger than 4 nm display similar detection efficiency curves. However, Hyytiälä ambient particles and alpha-pinene oxidation particles smaller than 4 nm require higher DEG saturator flow rates for activation than metal particles. The composition of sub-10 nm particles as well as the corresponding properties will affect the calibration results of PSM 2.0.

3.3 Ambient particle size distribution measurement

We used During the field campaign, 4 NPF events in Hyytiälä that happened were observed between 8 and 11 May,. The results measured by PSM 2.0 were and compared the particle size distributions inverted using different calibration files. Subsequently, these inverted size distributions by the PSM 2.0 were compared with the DMPS.

3.3.1 Total concentrations of 3-10 nm particles

Three calibration curves based on tungsten particles, Helsinki atmospheric particles, and Hyytiälä atmospheric particles are were used for the data inversion. The upper size limit for all three calibrations exceeds 10 nm. Obviously, PSM 2.0 is capable

330 ~~for the measurement of particles close to 1 nm, as displayed in the result of metal particles (Fig. 5).~~ Regarding the selection of 3 nm, PSM 2.0 clearly demonstrates the ability to measure particles as small as 1 nm, as shown in the metal particle results (Fig. 5). However, when performing direct calibration by using atmospheric particles, there is an insufficient signal intensity for sub-3 nm particles.

~~However, there was a lack of signal intensity when performing the calibration using ambient p~~

335 ~~articles. As displayed in Fig. S1-S3, under the condition of low sub-3 nm particle concentrations, it is hard to identify the presence of plateau concentrations as well as fitting the detection efficiency curves. As a result, t~~The lower size limits differ for different calibration files: for metal particles, the calibration is performed down to 1 nm, while for Helsinki and Hyytiälä particles, the smallest detectable sizes for calibration experiments were around 2 and 3 nm, respectively. To compare the total concentrations inverted from different calibration files, we selected a common measurement size range of 3-10 nm (Fig. 6).

340 (a)
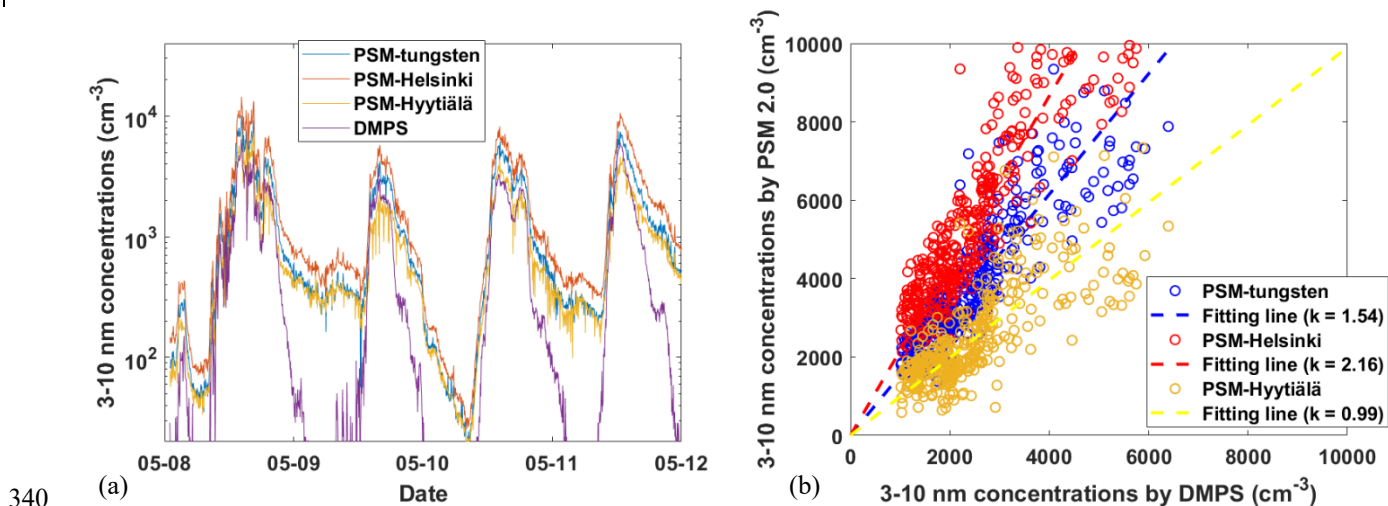
Figure 6. (a) 3-10 nm particle concentrations by PSM 2.0 and DMPS. Different types of particles were used for PSM 2.0 data inversion. (b) Comparison of total concentrations (sized between 3.1 to 10.1 nm) measured by DMPS and PSM 2.0 using different calibration methods. Only the DMPS total concentration results exceeding 1000 cm^{-3} are shown. The fitting line is based on the scattered data. A good correlation between PSM 2.0 and DMPS was observed, when Hyytiälä atmospheric particles was used for
345 **PSM 2.0 calibration.**

During the NPF events, high concentrations of 3-10 nm particles were observed. The total concentrations of 3-10 nm particles ~~measured by PSM 2.0 and DMPS were~~ are displayed in Fig. 6(a). The total concentrations ~~measured~~ by PSM and DMPS ~~were~~ are scattered, when the total concentrations measured by DMPS were higher than 1000 cm^{-3} (Fig. 6(b)). The best alignment between DMPS and PSM 2.0 measurements ~~occurred~~ occurs when using the Hyytiälä atmospheric particle calibration,
350 showing a slope close to 1 in the linear regression analysis. In-situ calibration provides the most accurate total concentration measurements. In contrast, the ~~other two~~ calibration files of tungsten particle and Helsinki ambient particle ~~resulted~~ result in overestimations ~~of~~ by a factor of 1.54 and 2.16, respectively. ~~This suggests that the calibration significantly influences the discrepancy in particle concentration between PSM and DMPS measurements.~~

14

However, during non-NPF events, when total concentrations of sub-10 nm particles were lower than 1000 cm^{-3}, the concentrations measured by DMPS were significantly lower than those measured by PSM 2.0. In this condition, PSM 2.0 can provide more reliable measurements than DMPS. This is because two instruments have different minimum concentration detection limit. The PSM can count single particles, resulting in a very low minimum concentration detection limit. Although sizing with PSM 2.0 is influenced by factors such as chemical composition, charging state, and relative humidity, the associated measurement uncertainties do not increase as concentrations decrease. PSM 2.0 can provide reliable total concentrations in both high and low ambient particle concentrations. In contrast, accurate measurements by DMPS require size-resolved particle concentrations to be above the minimum detection limit (Kangasluoma and Kontkanen, 2017). For sub-10 nm particles, both the charge fraction of nanoparticles in the neutralizer and the penetration efficiency through each component of the DMPS are low. The DMPS has a higher minimum concentration detection limit than PSM 2.0; if this limit is not met, its CPC may fail to detect any signal, leading to an underestimation of measured concentrations. This issue was particularly evident during our Hyytiälä campaign, where clean atmospheric conditions resulted in low sub-10 nm particle concentrations during non-NPF events. Consequently, ~~This is because~~ PSM is more suitable for measuring low concentrations of nanoparticles. ~~DMPS tends to underestimate concentrations,~~. ~~particularly as particle size decreases. This underestimation occurs because the penetration efficiency of nanoparticles in the DMPS is significantly affected by the processes of charging, classification, transport, and detection. Consequently, the concentrations measured by DMPS are often underestimated.~~
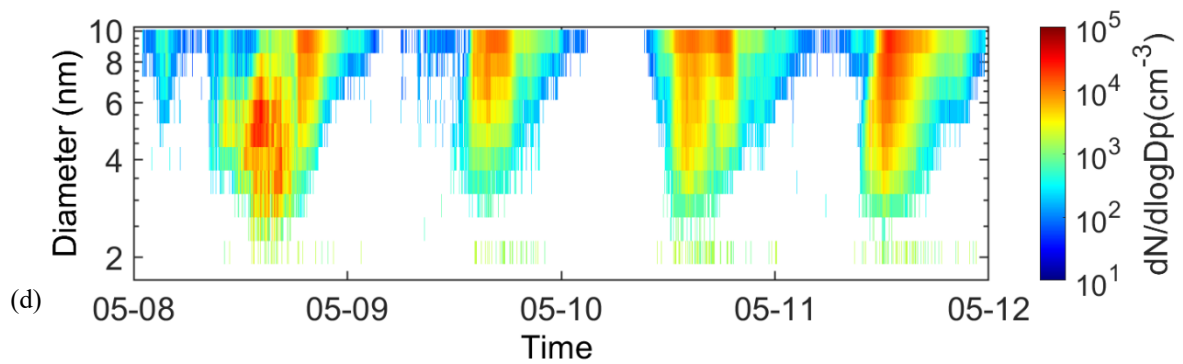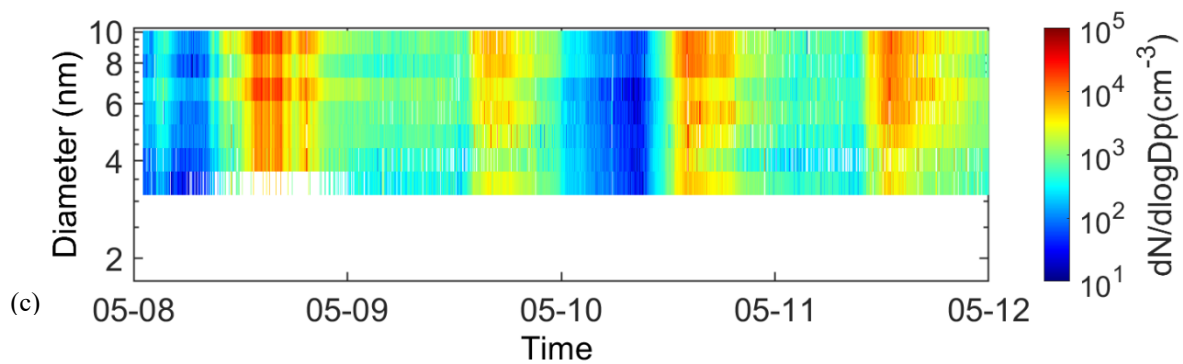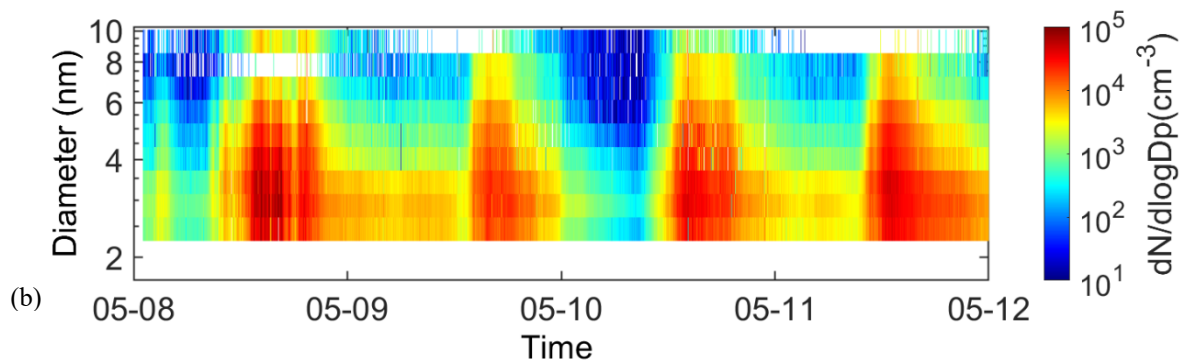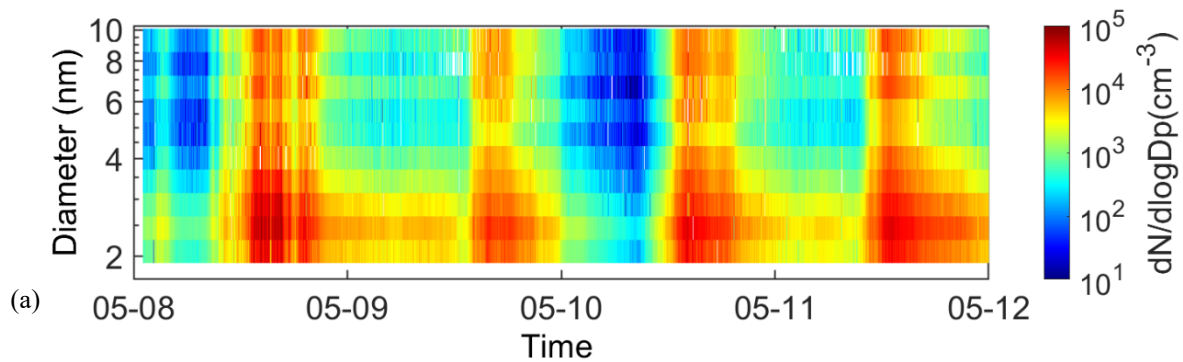
3.3.2 Particle number size distributions measured by PSM 2.0

~~The inverted particle number size distributions by PSM 2.0 were determined by the calibration file. Calibration of PSM 2.0 using atmospheric particles from Hyytiälä was limited to a minimum size of 3 nm. We selected the common size range across two instruments, and conducted an intercomparison.~~ The total concentrations were distributed into different size bins based on differernt calibration files. The ~~overall~~ inverted size distributions measured by PSM 2.0 and DMPS were displayed in Fig. 7. ~~Significant differences were observed when different calibrations being used. We selected the common size range across two instruments, and conducted an intercomparison.~~

Significant differences were observed in the inverted particle size distributions of PSM 2.0 when using different calibration files. When the calibration files for tungsten particles or Helsinki ambient particles were applied, the size-resolved concentrations showed an increasing trend as particle size decreased. In contrast, the opposite trend was observed when using the in-situ calibration file for Hyytiälä atmospheric particles. The validity of the in-situ calibration was confirmed through comparisons with DMPS measurements, which displayed a similar pattern in the 3-10 nm size range.

~~DMPS showed similar pattern in 3-10 nm with the PSM 2.0 by using the calibration obtained with Hyytiälä atmospheric particles. In contrast, the calibration based on tungsten and Helsinki atmospheric particles revealed an opposite trend.~~
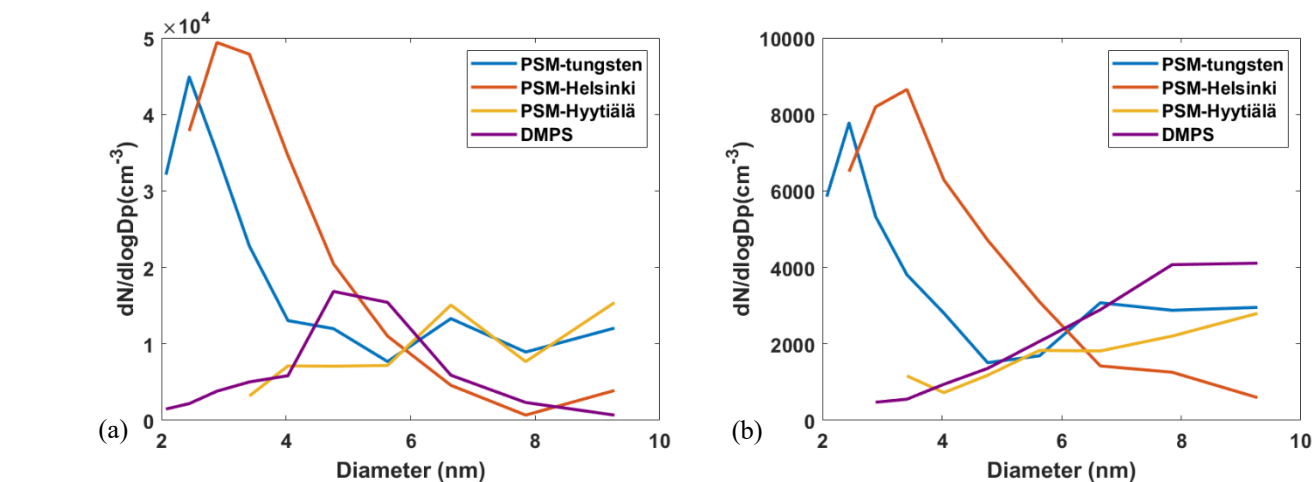
385

Figure 7. (a) Number size distributions measured by PSM 2.0 using the calibration of tungsten particles. (b) Number size distributions measured by PSM 2.0 using the calibration of Helsinki ambient particles. (c) Number size distributions measured by PSM 2.0 using the calibration of Hyytiälä ambient particles. (d) Number size distributions measured by DMPS.

To enhance the clarity of the intercomparison, we compared the mean number size distributions measured during four NPF events (from 13:00 to 15:00) (Fig. 8). Our result suggests that the inverted particle size distributions are sensitive to the calibrations. In the sub-3 nm size range, PSM 2.0 measurements using the calibration for tungsten particles and Helsinki ambient particles exhibited higher concentrations compared to DMPS results. As displayed in Fig. 5, the Hyytiälä atmospheric particles would need a higher DEG saturator flow rate to be activated. By using the wrong calibration file, the ambient particles larger than 3 nm were wrongly attributed to sub-3 nm size range, which caused the overestimation of sub-3 nm particles.

In four NPF events, three events (from 9 to 11 May) exhibited a similar particle size distribution pattern between DMPS and PSM 2.0 using the Hyytiälä atmospheric particle calibration, except for the event on 8 May. During that event, DMPS showed a peak concentration between 4-6 nm, with a noticeable decrease in concentration as particle size increased. Due to PSM 2.0''s lower size resolution in this range compared to DMPS, the measured particle size distribution tended to flatten out.

We do not assert that the results displayed by DMPS are absolutely accurate, as DMPS itself is subject to inherent uncertainties. However, within the size range of 3-10 nm, DMPS (and SMPS) is the most widely used instrument, and its sizing is based on electrical mobility classification, and theoritically ~~more~~ accurate and reliable. Meanwhile, PSM 2.0 can provide comparable particle size distributions in this size range. Considering PSM 2.0 and DMPS are based on different working principles, this consistency is noteworthy. This study offers a plausible explanation for the overestimation by PSM in the sub-4 nm size range in other studies, as well as the higher concentrations compared to DMPS.
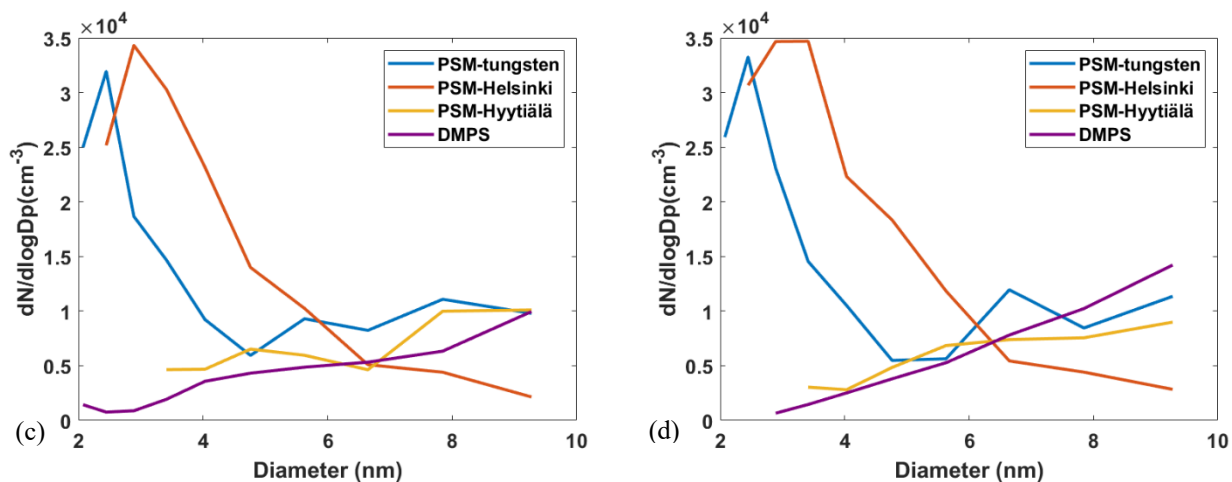

17

Figure 8. Mean number size distributions measured by PSM 2.0 and DMPS. The calibration of PSM 2.0 was based on tungsten metal particles, Helsinki atmospheric particles, and Hyytiälä atmospheric particles, respectively. The size distributions were collected during NPF events that occurred (a) from 13:00 to 15:00 on 8 May, (b) from 13:00 to 15:00 on 9 May, (c) from 13:00 to 15:00 on 10 May, and (d) from 13:00 to 15:00 on 11 May.

4. Conclusions

In this study, we calibrated the PSM 2.0 using different types of particles including tungsten particles, Ni/Cr particles, alpha-pinene oxidation particles, and atmospheric particles from Helsinki and Hyytiälä, respectively. Number size distributions of sub-10 nm particles based on different calibrations were investigated and compared with those measured by a DMPS. Calibration with Helsinki ambient particles showed a similar trend to metal particles, possibly because the composition of urban particles has the similar activation behaviour with metal particles. However, the activation of Hyytiälä ambient particles required higher DEG saturator flow rates than other types of particles. This difference underscores the significance of particle composition in calibration processes. Proper calibration enables PSM 2.0 to enhance its reliability. After in-situ calibration (using ~~Hyytiälä~~ the same atmospheric particles for calibration and subsequent measurements), PSM 2.0 exhibited a good correlation with DMPS in terms of both total concentrations and particle size distributions, particularly during NPF events. However, using a wrong calibration will lead to deviations in ~~the inversion results~~both the inverted total concentrations and particle size distributions. PSM 2.0 also showed its effectiveness in measuring low concentrations of sub-10 nm particles. The lower size limit for direct calibration using atmospheric particles was between 2 and 3 nm, primarily due to observed NPF events not strong enough and a lack of particle concentration after DMA classification. ~~This study did not perform in-situ PSM 2.0 calibration using particles close to 1 nm due to the NPF events not being strong enough. Such~~ More direct calibrations in differernt places around the world are expected in the future to further reduce the measurement uncertainty of PSM 2.0.

410

415

420

425

430

18

Code/Data availability

The characterizations of the tested PSM 2.0 are shown in the figures. The codes for the inversion methods are available upon request.

Author contribution

435   JK and YL designed the experiments. YL, AY, FS, and LA carried them out. YL prepared the manuscript with contributions from all co-authors.

Competing interests

The authors declare that they have no conflict of interest.

Disclaimer

440   Publisher's note: Copernicus Publications remains neutral with regard to jurisdictional claims made in the text, published maps, institutional affiliations, or any other geographical representation in this paper. While Copernicus Publications makes every effort to include appropriate place names, the final responsibility lies with the authors

References

Ahonen, L. R., Kangasluoma, J., Lammi, J., Lehtipalo, K., Hämeri, K., Petäjä, T., and Kulmala, M.: First measurements of the number size distribution of 1–2 nm aerosol particles released from manufacturing processes in a cleanroom environment, Aerosol Sci. Technol., 51, 685–693, https://doi.org/10.1080/02786826.2017.1292347, 2017.

450   Attoui, M., Perez-Lorenzo, L. J., Brock, C. A., and Fernández de la Mora, J.: High resolution characterization of a sheathed axisymmetric variable supersaturation condensation particle sizer, J. Aerosol Sci., 169, 106112, https://doi.org/10.1016/j.jaerosci.2022.106112, 2023.

Cai, R., Attoui, M., Jiang, J., Korhonen, F., Hao, J., Petäjä, T., and Kangasluoma, J.: Characterization of a high-resolution supercritical differential mobility analyzer at reduced flow rates, Aerosol Sci. Technol., 52, 1332–1343,
455   https://doi.org/10.1080/02786826.2018.1520964, 2018a.

Cai, R., Yang, D., Ahonen, L. R., Shi, L., Korhonen, F., Ma, Y., Hao, J., Petäjä, T., Zheng, J., Kangasluoma, J., and Jiang, J.: Data inversion methods to determine sub-3 nm aerosol size distributions using the particle size magnifier, Atmos Meas Tech, 11, 4477–4491, https://doi.org/10.5194/amt-11-4477-2018, 2018b.

460 Chan, T., Cai, R., Ahonen, L. R., Liu, Y., Zhou, Y., Vanhanen, J., Dada, L., Chao, Y., Liu, Y., Wang, L., Kulmala, M., and Kangasluoma, J.: Assessment of particle size magnifier inversion methods to obtain the particle size distribution from atmospheric measurements, Atmos Meas Tech, 13, 4885–4898, https://doi.org/10.5194/amt-13-4885-2020, 2020.

Fernández de la Mora, J.: Expanded flow rate range of high-resolution nanoDMAs via improved sample flow injection at the aerosol inlet slit, J Aerosol Sci, 113, 265–275, https://doi.org/10.1016/j.jaerosci.2017.07.020, 2017.

Fernández de la Mora, J., Kangasluoma, J., and Attoui, M.: Size resolution of the Airmodus A10 particle size magnifier with 465 purified clusters, J. Aerosol Sci., 160, 105916, https://doi.org/10.1016/j.jaerosci.2021.105916, 2022.

Iida, K., Stolzenburg, M. R., and McMurry, P. H.: Effect of Working Fluid on Sub-2 nm Particle Detection with a Laminar Flow Ultrafine Condensation Particle Counter, Aerosol Sci Tech, 43, 81–96, https://doi.org/10.1080/02786820802488194, 2011.

Jiang, J., Chen, M., Kuang, C., Attoui, M., and McMurry, P. H.: Electrical Mobility Spectrometer Using a Diethylene Glycol 470 Condensation Particle Counter for Measurement of Aerosol Size Distributions Down to 1 nm, Aerosol Sci. Technol., 45, 510–521, https://doi.org/10.1080/02786826.2010.547538, 2011.

Kangasluoma, J. and Kontkanen, J.: On the sources of uncertainty in the sub-3nm particle concentration measurement, J. Aerosol Sci., 112, 34–51, https://doi.org/10.1016/j.jaerosci.2017.07.002, 2017.

Kangasluoma, J., Junninen, H., Lehtipalo, K., Mikkilä, J., Vanhanen, J., Attoui, M., Sipilä, M., Worsnop, D., Kulmala, M., 475 and Petäjä, T.: Remarks on Ion Generation for CPC Detection Efficiency Studies in Sub-3-nm Size Range, Aerosol Sci Tech, 47, 556–563, https://doi.org/10.1080/02786826.2013.773393, 2013.

Kangasluoma, J., Kuang, C., Wimmer, D., Rissanen, M. P., Lehtipalo, K., Ehn, M., Worsnop, D. R., Wang, J., Kulmala, M., and Petäjä, T.: Sub-3 nm particle size and composition dependent response of a nano-CPC battery, Atmos Meas Tech, 7, 689–700, https://doi.org/10.5194/amt-7-689-2014, 2014.

480 Kangasluoma, J., Attoui, M., Junninen, H., Lehtipalo, K., Samodurov, A., Korhonen, F., Sarnela, N., Schmidt-Ott, A., Worsnop, D., Kulmala, M., and Petäjä, T.: Sizing of neutral sub 3nm tungsten oxide clusters using Airmodus Particle Size Magnifier, J. Aerosol Sci., 87, 53–62, https://doi.org/10.1016/j.jaerosci.2015.05.007, 2015.

Kangasluoma, J., Samodurov, A., Attoui, M., Franchin, A., Junninen, H., Korhonen, F., Kurtén, T., Vehkamäki, H., Sipilä, M., Lehtipalo, K., Worsnop, D. R., Petäjä, T., and Kulmala, M.: Heterogeneous Nucleation onto Ions and Neutralized Ions: 485 Insights into Sign-Preference, J Phys Chem C, 120, 7444–7450, https://doi.org/10.1021/acs.jpcc.6b01779, 2016a.

Kangasluoma, J., Franchin, A., Duplissy, J., Ahonen, L., Korhonen, F., Attoui, M., Mikkilä, J., Lehtipalo, K., Vanhanen, J., Kulmala, M., and Petäjä, T.: Operation of the Airmodus A11 nano Condensation Nucleus Counter at various inlet pressures and various operation temperatures, and design of a new inlet system, Atmos Meas Tech, 9, 2977–2988, https://doi.org/10.5194/amt-9-2977-2016, 2016b.

Kangasluoma, J., Ahonen, L. R., Laurila, T. M., Cai, R., Enroth, J., Mazon, S. B., Korhonen, F., Aalto, P. P., Kulmala, M., Attoui, M., and Petäjä, T.: Laboratory verification of a new high flow differential mobility particle sizer, and field measurements in Hyytiälä, J. Aerosol Sci., 124, 1–9, https://doi.org/10.1016/j.jaerosci.2018.06.009, 2018.

Kangasluoma, J., Cai, R., Jiang, J., Deng, C., Stolzenburg, D., Ahonen, L. R., Chan, T., Fu, Y., Kim, C., Laurila, T. M., Zhou, Y., Dada, L., Sulo, J., Flagan, R. C., Kulmala, M., Petäjä, T., and Lehtipalo, K.: Overview of measurements and current instrumentation for 1–10 nm aerosol particle number size distributions, J. Aerosol Sci., 148, 105584, https://doi.org/10.1016/j.jaerosci.2020.105584, 2020.

Keshavarz, F., Kubečka, J., Attoui, M., Vehkamäki, H., Kurtén, T., and Kangasluoma, J.: Molecular Origin of the Sign Preference of Ion- Induced Heterogeneous Nucleation in a Complex Ionic Liquid–Diethylene Glycol System, J. Phys. Chem. C, 124, 26944–26952, https://doi.org/10.1021/acs.jpcc.0c09481, 2020a.

Keshavarz, F., Kurtén, T., Vehkamäki, H., and Kangasluoma, J.: Seed–Adsorbate Interactions as the Key of Heterogeneous Butanol and Diethylene Glycol Nucleation on Ammonium Bisulfate and Tetramethylammonium Bromide, J. Phys. Chem. A, 124, 10527–10539, https://doi.org/10.1021/acs.jpca.0c08373, 2020b.

Kim, C. S., Okuyama, K., and Fernández de la Mora, J.: Performance Evaluation of an Improved Particle Size Magnifier (PSM) for Single Nanoparticle Detection, Aerosol Sci. Technol., 37, 791–803, https://doi.org/10.1080/02786820300913, 2003.

Kogan, Ya. I. and Burnasheva, Z. A.: Growth and Measurement of Condensation Nuclei in a Continuous Stream, Russian Journal of Physical Chemistry, 34, 1960.

Kulmala, M., Mordas, G., Petäjä, T., Grönholm, T., Aalto, P. P., Vehkamäki, H., Hienola, A. I., Herrmann, E., Sipilä, M., Riipinen, I., Manninen, H. E., Hämeri, K., Stratmann, F., Bilde, M., Winkler, P. M., Birmili, W., and Wagner, P. E.: The condensation particle counter battery (CPCB): A new tool to investigate the activation properties of nanoparticles, J Aerosol Sci, 38, 289–304, https://doi.org/10.1016/j.jaerosci.2006.11.008, 2007.

Kulmala, M., Kontkanen, J., Junninen, H., Lehtipalo, K., Manninen, H. E., Nieminen, T., Petäjä, T., Sipilä, M., Schobesberger, S., Rantala, P., Franchin, A., Jokinen, T., Järvinen, E., Äijälä, M., Kangasluoma, J., Hakala, J., Aalto, P. P., Paasonen, P., Mikkilä, J., Vanhanen, J., Aalto, J., Hakola, H., Makkonen, U., Ruuskanen, T., Mauldin, R. L., Duplissy, J., Vehkamäki, H., Bäck, J., Kortelainen, A., Riipinen, I., Kurtén, T., Johnston, M. V., Smith, J. N., Ehn, M., Mentel, T. F., Lehtinen, K. E. J., Laaksonen, A., Kerminen, V.-M., and Worsnop, D. R.: Direct Observations of Atmospheric Aerosol Nucleation, Science, 339, 943–946, https://doi.org/10.1126/science.1227385, 2013.

Lehtipalo, K., Ahonen, L. R., Baalbaki, R., Sulo, J., Chan, T., Laurila, T., Dada, L., Duplissy, J., Miettinen, E., Vanhanen, J., Kangasluoma, J., Kulmala, M., Petäjä, T., and Jokinen, T.: The standard operating procedure for Airmodus Particle Size Magnifier and nano-Condensation Nucleus Counter, J Aerosol Sci, 159, 105896, https://doi.org/10.1016/j.jaerosci.2021.105896, 2021.

Li, X., Li, Y., Cai, R., Yan, C., Qiao, X., Guo, Y., Deng, C., Yin, R., Chen, Y., Li, Y., Yao, L., Sarnela, N., Zhang, Y., Petäjä, T., Bianchi, F., Liu, Y., Kulmala, M., Hao, J., Smith, J. N., and Jiang, J.: Insufficient Condensable Organic Vapors Lead to Slow Growth of New Particles in an Urban Environment, Environ Sci Technol, 56, 9936–9946, https://doi.org/10.1021/acs.est.2c01566, 2022.

Liu, Y., Attoui, M., Yang, K., Chen, J., Li, Q., and Wang, L.: Size-resolved chemical composition analysis of ions produced by a commercial soft X-ray aerosol neutralizer, J Aerosol Sci, 147, 105586, https://doi.org/10.1016/j.jaerosci.2020.105586, 2020.

530 Liu, Y., Attoui, M., Li, Y., Chen, J., Li, Q., and Wang, L.: Factors that govern sub-3 nm particle measurements in an Airmodus® PSM and a TSI ® DEG-SMPS, Aerosol Sci Tech, 1–14, https://doi.org/10.1080/02786826.2022.2098686, 2022.

Liu, Y., Attoui, M., Baalbaki, R., Cai, R., Biskos, G., Chen, Y., and Kangasluoma, J.: Number size distribution and charging properties of sub-10 nm metal-based particles produced by spark ablation at atmospheric pressure, Aerosol Sci. Technol., ahead-of-print, 1–13, https://doi.org/10.1080/02786826.2024.2355174, 2024.

Okuyama, K., Kousaka, Y., and Motouchi, T.: Condensational Growth of Ultrafine Aerosol Particles in a New Particle Size
535 Magnifier, Aerosol Sci. Technol., 3, 353–366, https://doi.org/10.1080/02786828408959024, 1984.

Rönkkö, T., Kuuluvainen, H., Karjalainen, P., Keskinen, J., Hillamo, R., Niemi, J. V., Pirjola, L., Timonen, H. J., Saarikoski, S., Saukko, E., Järvinen, A., Silvennoinen, H., Rostedt, A., Olin, M., Yli-Ojanperä, J., Nousiainen, P., Kousa, A., and Maso, M. D.: Traffic is a major source of atmospheric nanocluster aerosol, Proc National Acad Sci, 114, 7549–7554, https://doi.org/10.1073/pnas.1700830114, 2017.

540 Sgro, L. A. and Fernández de la Mora, J.: A Simple Turbulent Mixing CNC for Charged Particle Detection Down to 1.2 nm, Aerosol Sci. Technol., 38, 1–11, https://doi.org/10.1080/02786820490247560, 2004.

Sulo, J., Enroth, J., Pajunoja, A., Vanhanen, J., Lehtipalo, K., Petäjä, T., and Kulmala, M.: Pushing nano-aerosol measurements towards a new decade – technical note on the Airmodus particle size magnifier 2.0, Aerosol Res., 2, 13–20, https://doi.org/10.5194/ar-2-13-2024, 2024.

545 Toropainen, A., Kangasluoma, J., Kurtén, T., Vehkamäki, H., Keshavarz, F., and Kubečka, J.: Heterogeneous Nucleation of Butanol on NaCl: A Computational Study of Temperature, Humidity, Seed Charge, and Seed Size Effects, J. Phys. Chem. A, 125, 3025–3036, https://doi.org/10.1021/acs.jpca.0c10972, 2021.

Vanhanen, J., Mikkilä, J., Lehtipalo, K., Sipilä, M., Manninen, H. E., Siivola, E., Petäjä, T., and Kulmala, M.: Particle Size Magnifier for Nano-CN Detection, Aerosol Sci. Technol., 45, 533–542, https://doi.org/10.1080/02786826.2010.547889,
550 2011.

Wiedensohler, A. and Fissan, H. J.: Bipolar Charge Distributions of Aerosol Particles in High-Purity Argon and Nitrogen, Aerosol Sci Tech, 14, 358–364, https://doi.org/10.1080/02786829108959498, 1991.

Winkler, P. M., Steiner, G., Vrtala, A., Vehkamäki, H., Noppel, M., Lehtinen, K. E. J., Reischl, G. P., Wagner, P. E., and Kulmala, M.: Heterogeneous Nucleation Experiments Bridging the Scale from Molecular Ion Clusters to Nanoparticles,
555 Science, 319, 1374–1377, https://doi.org/10.1126/science.1149034, 2008.

Wlasits, P. J., Stolzenburg, D., Tauber, C., Brilke, S., Schmitt, S. H., Winkler, P. M., and Wimmer, D.: Counting on chemistry: laboratory evaluation of seed-material-dependent detection efficiencies of ultrafine condensation particle counters, Atmos Meas Tech, 13, 3787–3798, https://doi.org/10.5194/amt-13-3787-2020, 2020.

Yao, L., Garmash, O., Bianchi, F., Zheng, J., Yan, C., Kontkanen, J., Junninen, H., Mazon, S. B., Ehn, M., Paasonen, P.,
560 Sipilä, M., Wang, M., Wang, X., Xiao, S., Chen, H., Lu, Y., Zhang, B., Wang, D., Fu, Q., Geng, F., Li, L., Wang, H., Qiao, L., Yang, X., Chen, J., Kerminen, V.-M., Petäjä, T., Worsnop, D. R., Kulmala, M., and Wang, L.: Atmospheric new particle

formation from sulfuric acid and amines in a Chinese megacity, Science, 361, 278–281, https://doi.org/10.1126/science.aao4839, 2018.

565